NMR, EPR, and bulk susceptibility measurements of one-dimensional $SrNbO_{3.41}$

J.-E. Weber, C. Kegler, N. Büttgen, H.-A. Krug von Nidda, and A. Loidl
Experimentalphysik V, Elektronische Korrelationen und Magnetismus, Institut für Physik, Universität Augsburg, D-86135 Augsburg, Germany

F. Lichtenberg
Experimentalphysik VI, Elektronische Korrelationen und Magnetismus, Institut für Physik, Universität Augsburg, D-86135 Augsburg, Germany

(Received 1 June 2001; revised manuscript received 28 August 2001; published 27 November 2001)

NMR, EPR, and bulk susceptibility measurements were performed in the perovskite-related layered compound $SrNbO_{3.41}$. We determined ^{93}Nb NMR spectra, spin-spin relaxation rates $1/T_2$ and spin-lattice relaxation rates $1/T_1$ down to 600 mK. From the spin-lattice relaxation $1/T_1$ we identified an activated behavior $1/T_1 \propto \exp(-\Delta_{NMR}/k_BT)$ with a gap $\Delta_{NMR}=6.5$ meV for temperatures $T>20$ K. Below 20 K, the line width $\Delta H(T)$ from acceptor-EPR and $^{93}(1/T_1)(T)$ both exhibit a temperature dependence propotional to $\exp[-(T_0/T)^{1/2}]$ which is indicative for a variable range hopping process. We discuss the possibility of charge-density-wave formation at low temperatures.

DOI: 10.1103/PhysRevB.64.235414 PACS number(s): 71.30.+h, 73.90.+f, 76.60.Es, 76.30.He

I. INTRODUCTION

Perovskite-related layered niobates belonging to the homologous series $A_nB_nO_{3n+2}$ such as $SrNbO_{3.45}$ ($n=4.5$) and $SrNbO_{3.4}$ ($n=5$) gained considerable interest after reports on one-dimensional (1D) metallic behavior.[1–3] Their structure is derived from the three-dimensional network of the ABO_3 perovskite structure by introducing additional oxygen and thereby separating the BO_6 octahedra parallel to the (110) planes resulting in NbO_6 octahedra which are chainlike connected along the crystallographic a axis.[3–5] By tuning the oxygen content in $SrNbO_{3.5-x}$ one can synthesize compounds with interesting properties: The fully oxidized $n=4$ compound $SrNbO_{3.5}$ is a layered ferroelectric with one of the highest ferroelectric transition temperatures ($=1615$ K) reported so far.[6,7] With decreasing oxygen content a superlattice arises for $SrNbO_{3.45}$ ($n=4.5$) which is formed by well ordered stacking sequences of $n=4$ and $n=5$ subunits.[3,4] For $x\approx 0.1$ there are compounds with $n=5$ within the homogeneity range from $SrNbO_{3.42}$ to $SrNbO_{3.40}$.[3,4]

Angle-resolved photoemission, submillimeter and far infrared spectroscopy, and resistivity measurements revealed that $SrNbO_{3.41}$ is a one-dimensional metal.[2,3,8] Also LDA band-structure calculations agree with this experimentally detected anisotropy of the electronic properties and indicate discernible electronic dispersion along the a axis, only.[1] A high dielectric polarizibility and a tendency for polaron formation has been detected by dielectric spectroscopy along the c axis.[9] In these dielectric experiments on $SrNbO_{3.41}$ a phase transition of so far unknown origin has been found close to room temperature. With decreasing temperature, the above mentioned experimental investigations also established a metal-to-semiconductor transition at $T\approx 40$ K opening a small excitation gap of a few meV in size.[2,3] The microscopic origin of this gapping of the Fermi surface is still unclear and it might be necessary to take into consideration a structural phase transition or electronic correlations inducing the observed gap. Certainly, the one-dimensional behavior evokes speculations about the formation of a charge-density wave (CDW).

Here, we present a detailed study of the one-dimensional conductor $SrNbO_{3.41}$ utilizing bulk magnetization measurements and magnetic resonance techniques. Single crystals of $SrNbO_{3.41}$ with lattice parameters $a=3.99$ Å, $b=5.67$ Å, and $c=32.45$ Å were prepared from the constituents Nb_2O_5 (purity 99.9%), Nb powder (99.9%), and $SrCO_3$ (>99%) by floating zone melting as described in detail by Lichtenberg *et al.*[3] All measurements were performed on single crystalline pieces from the same batch. For some NMR experiments the single crystals were crushed into powders.

II. EXPERIMENTAL DETAILS AND RESULTS

A. Magnetic susceptibility

The dc magnetization $M(T)$ was determined using a commercial SQUID magnetometer from Quantum Design in an external field of 10 kOe for temperatures $1.8<T<380$ K. In the complete temperature range, the susceptibility $\chi = M(T)/H$, shown in Fig. 1, turned out to be negative demonstrating that diamagnetic contributions dominate. Starting at the highest temperatures, χ exhibits an almost temperature independent plateau down to 250 K. On further decreasing temperatures the susceptibility decreases monotonically down to 50 K and increases again with a Curie-Weiss-type behavior towards the lowest temperature of 1.8 K.

The anisotropic electronic character of $SrNbO_{3.41}$ is well established by the observation of one-dimensional metallic behavior along the a axis for $60<T<130$ K followed by a regime with increasing resistivity towards the lowest temperatures, and by a semiconducting characteristic along the b and c axis within the whole temperature range.[2,3] Having these facts in mind, two models could be used to analyze the suceptibility data in Fig. 1. In a first approach we assume that $\chi(T)$ is dominated by thermally activated charge carriers and try the ansatz

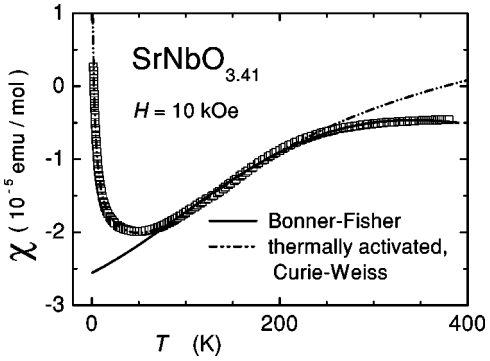

FIG. 1. Magnetic susceptibility $\chi(T)$ for temperatures $1.8<T<380$ K, measured in an external magnetic field of 10 kOe. Dotted line: Pauli paramagnetism of thermally activated charge carriers across an energy gap of $E_g=19.8$ meV at elevated temperatures and a Curie-Weiss contribution of defect states at low temperatures according to Eq. (1). Solid line: One-dimensional $S=1/2$ Heisenberg AFM chain with an exchange constant $|J|=530$ K following Ref. 13 according to Eq. (2).

$$\chi(T)=\chi_{\mathrm{dia}}+\frac{C}{T-\theta}+\chi_{\mathrm{Pauli}}\exp\left(-\frac{E_g}{k_BT}\right). \tag{1}$$

The first term represents the diamagnetic contribution of closed electron shells. The second term reflects the Curie-Weiss tail of defect states at low temperatures. The third term describes the Pauli paramagnetism from thermally activated charge carriers which are excited across an energy gap E_g into the conduction band. The dashed line in Fig. 1 represents the best fit to the experimental data using Eq. (1). The diamagnetic contribution $\chi_{\mathrm{dia}}=-2.2\times10^{-5}$ emu/mol seems to be somewhat too low when compared to the diamagnetism $\chi_{\mathrm{dia}}=-6.5\times10^{-5}$ emu/mol, determined from the summation of the ionic constituents $Sr^{2+}(-15)$, $Nb^{5+}(-9)$, and $O^{2-}(-12)$. The values in brackets denote the diamagnetic susceptibilities in units of 10^{-6} emu/mol.[10] The low temperature tail, indicative for defect spins, exhibits a Curie-Weiss constant $C=9.9\times10^{-5}$K emu/mol and an antiferromagnetic Curie-Weiss temperature $\theta=-2.1$ K. Assuming defects with spin $S=1/2$, we deduce an impurity concentration of 0.03% per formula unit as an upper limit. EPR experiments performed in the above mentioned starting materials identified traces of $Fe^{3+}(S=5/2)$ in Nb_2O_5 and $Mn^{2+}(S=5/2)$ in $SrCO_3$. Due to these large spin values, the real impurity concentration might be an order of magnitude smaller. The saturated Pauli paramagnetism of the charge carriers amounts $\chi_{\mathrm{Pauli}}=4.1\times10^{-5}$ emu/mol. The temperature regime $50\leqslant T\leqslant200$ K is well reproduced assuming activation processes across an energy gap of $E_g=19.8$ meV. The experimental susceptibility at room temperature is negative $\chi_{300\,\mathrm{K}}\approx-0.5\times10^{-5}$ emu/mol and clearly is overestimated by the fit results. Subtracting the theoretically estimated diamagnetic contribution $\chi_{\mathrm{dia}}=-6.5\times10^{-5}$ emu/mol, we obtain a value of $\chi=6\times10^{-5}$ emu/mol which resembles the Pauli spin susceptibility. We compare this value to the Pauli paramagnetism of elemental niobium $\chi_{\mathrm{Pauli}}=10.9\times10^{-5}$ emu/mol.[11] This hints towards an appreciable density of states at the Fermi level also for $SrNbO_{3.41}$ at room temperature.

In a second attempt to fit $\chi(T)$ as shown in Fig. 1, we focus on the one-dimensional (1D) electronic properties and try to fit the experimental results using the Bonner-Fisher model for the susceptibility $\chi_{1\mathrm{D}}$ of an 1D antiferromagnetic $S=1/2$ Heisenberg spin chain,[12] i.e.,

$$\chi_{1\mathrm{D}}(T)=\chi_{\mathrm{dia}}+\frac{V\Gamma}{T}\times\frac{0.25+0.0774975J/T+0.075235(J/T)^2}{1+0.9931J/T+0.172135(J/T)^2+0.757825(J/T)^3} \tag{2}$$

with $\Gamma=1.5012$ emu K/mol.[13] The prefactor V is the fraction of electrons per formula unit which contribute to the 1D spin chain. The parameter J describes the antiferromagnetic coupling between localized nearest-neighbor spins. Equation (2) is best applicable for temperatures $T\geqslant0.3J$.[13] Therefore, we restrict the fit using Eq. (2) to temperatures $50\leqslant T\leqslant400$ K leaving J,V, and χ_{dia} as fit parameters (solid line in Fig. 1). The exchange constant is rather high, namely, $J=530$ K, in accordance with strong intrachain interactions of neighboring spins. Large values of J are indicative of spin chains with the charges close to delocalization, in accordance with the experimental results mentioned in Sec. I that $SrNbO_{3.41}$ is a one-dimensional conductor along the *a* axis. The prefactor $V=0.15$ nicely resembles the expected value of 0.18 electrons per formula unit $SrNbO_{3.41}$ as it is obtained from charge neutrality. Astonishingly, the diamagnetic susceptibility $\chi_{\mathrm{dia}}=-6.8\times10^{-5}$ emu/mol is in extraordinary good agreement with the theoretical value mentioned above.

B. NUCLEAR MAGNETIC RESONANCE

1. ^{93}Nb spectra

The NMR measurements have been carried out with a phase-coherent pulse spectrometer probing the ^{93}Nb nuclei (spin $I=9/2$, gyromagnetic ratio $\gamma=10.406$ MHz/T). Cryogenic temperatures were provided by a ^{3}He/^{4}He dilution refrigerator from Oxford Instruments with the NMR resonant circuit residing in the mixing chamber and conventional ^{4}He techniques at elevated temperatures, respectively. Spectra were obtained by field sweeps at constant radio frequencies (rf) $\omega_0/2\pi=28$ MHz and $\omega_0/2\pi=45$ MHz for polycrystalline powder samples as well as for an arrangement of some single crystals, respectively. Four single crystals of different size were stacked together with the *c* axes being oriented perpendicular to the external field. The spectra were collected using a conventional 1.5 $\mu s-\tau_D-3$ μs spin-echo sequence ($\tau_D=50$ μs). The higher frequency of 45 MHz was needed in order to increase the nuclear signals of the tiny single crystals which only provided a poor filling factor of the resonance coil.

Figure 2 shows ^{93}Nb spectra for the polycrystalline sample at a radio frequency of 28 MHz and temperatures 2.3,

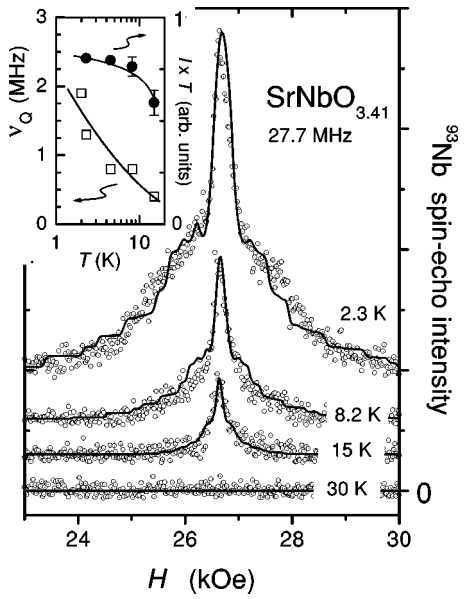

FIG. 2. ^{93}Nb NMR field-swept spectra for temperatures $2.3 < T < 30$ K. The solid lines indicate spectra simulations of the powder pattern for $I = 9/2$ nuclei at 27.7 MHz. Inset: temperature dependence of the quadrupole coupling frequency ν_Q, and the integrated intensity ($I \times T$) of the powder pattern. The lines in the inset are drawn to guide the eye.

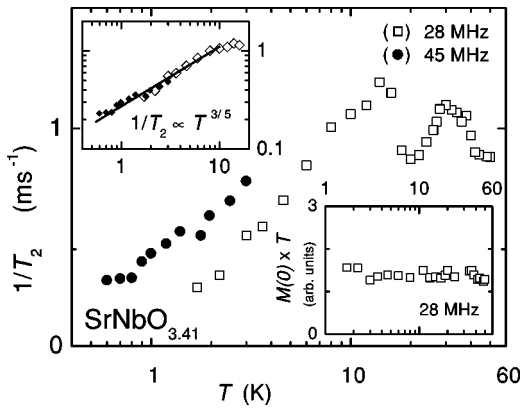

FIG. 3. Spin-spin relaxation rate $1/T_2$ vs $\ln T$. Stacked single crystals: /●/, $\omega_0 = 45$ MHz; polycrystalline powder: /□/, $\omega_0 = 28$ MHz. Upper inset: rescaled $1/T_2(T)$ data in double logarithmic representation. Solid line emphasizes the power law temperature dependence. Lower inset: intensity [$M(0) \times T$ in arbitrary units] of the spin-echo amplitude which was obtained from the T_2 decay for $\tau_D \to 0$.

8.2, 15, and 30 K. The spectra are composed of a pronounced central transition ($1/2 \leftrightarrow -1/2$) accompanied by an almost symmetric pedestal which appeared to be quadrupolar in origin due to the interaction between the electrical quadrupolar moment of the ^{93}Nb nuclei and the electrical field gradient (EFG) at the nuclear site.[11] The product of the integrated ^{93}Nb spin-echo intensity and temperature $I \times T$, which cancels the Curie-type contribution of the nuclear magnetization, is plotted in the inset of Fig. 2 (solid circles). With decreasing temperature, the area $I \times T$ of the spectra slightly increases. This signal increase most likely is due to the slowing down of the spin-spin relaxation $1/T_2(T)$ towards lower temperatures (see next section) which results in higher echo intensities at a fixed pulse separation τ_D (so called T_2 effect). From spectra simulations (the solid lines in Fig. 2) we obtained the quadrupole coupling frequency ν_Q and the asymmetry parameter $\eta \approx 0.5$ which determines the ratio of the EFG values along the principal axes of the electrostatic crystal potentials surrounding the probing nuclei.[11] It is important to note that the simulations exhibit a very narrow Gaussian broadening of the edge singularities of the satellite transitions which are not resolved in the experimental pattern. The quadrupole coupling frequency ν_Q reveals a significant temperature dependence (see open squares in the inset of Fig. 2). Such an increase of the quadrupole coupling frequency ν_Q towards lower temperatures, accompanied by a slowing down of the spin-spin relaxation process, was interpreted in terms of a fluctuating quadrupole field due to the formation of a CDW in the prototypical metallic linear-chain compound $NbSe_3$.[14] The spectra which were obtained using a number of oriented single crystals (not shown) could also be simulated using the same value of the asymmetry parameter $\eta \approx 0.5$ and assuming a preferential alignment of the principal axis with the strongest EFG being perpendicular to the external field. Within the entire temperature range the line shift of the central transition $K_{iso} \approx -0.15\%$ remains temperature independent pointing towards a temperature independent local susceptibility for $T < 15$ K which obviously is not affected by the Curie-Weiss-type susceptibility of the defect spins discussed above.

2. Spin-Spin relaxation T_2

The spin-spin relaxation rate $1/T_2$ was obtained by fitting the decay of the transverse magnetization

$$M(2\tau) = M(0)\exp\left(-\frac{2\tau}{T_2}\right) \tag{3}$$

as a function of the pulse separation time τ between the first and second rf pulses. The temperature dependence of the spin-spin relaxation rate $1/T_2$ is presented in Fig. 3 for frequencies $\omega_0 = 28$ MHz (solid circle) and $\omega_0 = 45$ MHz (open squares), respectively. The values of the spin-spin relaxation rate $1/T_2$ are found to scale linearly with frequency at constant temperatures, i.e., $1/T_2 \propto \omega_0$. In the upper inset of Fig. 3 we rescaled both data sets, i.e., we divided the data of 45 MHz by 1.6(=45 MHz/28 MHz) and left the data of 28 MHz as it is. The increase of $1/T_2(T)$ from low temperatures up to 15 K exhibits a power law dependence $1/T_2(T) \propto T^{3/5}$, followed by a relative minimum close $T = 20$ K and a relative maximum close to $T = 30$ K. The origin of these anomalies is not clear. A maximum in $1/T_2(T)$ has also been observed in the prototypical one-dimensional conductor $NbSe_3$ and has been attributed to dynamics of the quadrupole field caused by the CDW.[14] The transverse signal intensity $M(0)$ exhibits a pure Curie law within the entire temperature range. This is demonstrated by $M(0) \times T = \text{const}$ for $1.7 < T < 50$ K in the lower inset of Fig. 3. Hence, these anomalies in $1/T_2(T)$ cannot be attributed to extraneous signals of the

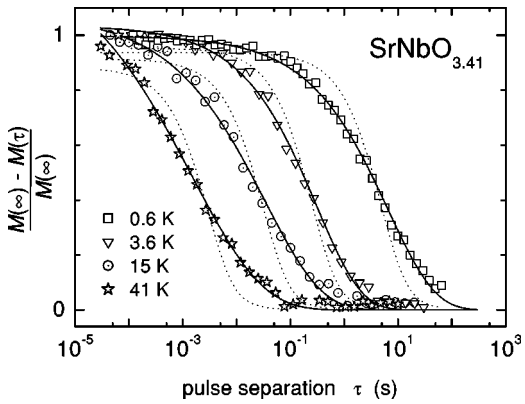

FIG. 4. Magnetization recovery vs pulse separation τ of the longitudinal relaxation process $1/T_1$ for 600 mK$<T<$41 K. Solid lines represent fits to Eq. (5). The dotted lines represent fits to Eq. (4).

pulsed T_2 experiment due to the recovery of the probe, i.e., coil ringing. All relaxation rates at elevated temperatures were obtained by extensive signal averaging which has been increased typically three orders of magnitude compared to the spectra measurements of Fig. 2.

3. Spin-lattice relaxation T_1

The experiments determining the spin-lattice relaxation rate $1/T_1$ were performed by irradiating the center field of the spectra and monitoring the inversion recovery of the longitudinal magnetization after a conventional three-pulse train. The recovery of the inverted central transition $(1/2 \leftrightarrow -1/2)$ for nuclear spin systems $I=9/2$ is theoretically expected to be of the pentaexponential form[15]

$$\frac{M(\infty)-M(\tau)}{M(\infty)} = 0.012\exp(-2W\tau) + 0.067\exp(-12W\tau) + 0.185\exp(-30W\tau) + 0.43\exp(-56W\tau) + 1.306\exp(-90W\tau), \quad (4)$$

where a unique relaxation rate $1/T_1$ can be deduced from the expression $2W=1/T_1$. The weight of each exponential term is obtained from the initial conditions of the spin-lattice relaxation process given in Ref. 16 for a selectively excited central transition. The results of the fit to Eq. (4) are indicated as dotted lines in Fig. 4 and it is to be seen that the accordance with the data is not satisfactory both at short and at long times. Due to huge quadrupole mixing ($\eta \approx 0.5$) the inversion efficiency of the central transition in our case is hard to determine and the unknown initial conditions leave at least six free parameters for the pentaexponential recovery in Eq. (4).[17] In order to simplify the description of the magnetization recovery and to put the number of fitting parameters to a minimum, we used a stretched exponential function

$$\frac{M(\infty)-M(\tau)}{M(\infty)} = \exp\left[-\left(\frac{\tau}{T_1}\right)^{\beta}\right] \quad (5)$$

which proved to describe our data within the entire temperature range $0.6<T<41$ K over six decades in time. The results are shown in Fig. 4 as solid lines. A stretched exponential often is used in systems characterized by a broad distribution of relaxation times in site-disordered or frustrated systems. As the pentaexponential recovery function also represents a distribution of five single exponential processes, a description of the recovery using Eq. (5) seems reasonable. The resulting temperature dependencies of the stretching exponent β and the spin-lattice relaxation rate $1/T_1$ which we take as a mean relaxation rate are shown in Fig. 5. We note that for $\beta<1$ the quantity $1/T_1$ is not a well-defined average rate and the observed value $0.3<\beta<0.5$ might be due to a distribution of spin-lattice relaxation times T_1 or spin diffusion processes of the nuclear spin system with a vanishingly small spin diffusion coefficient.[18]

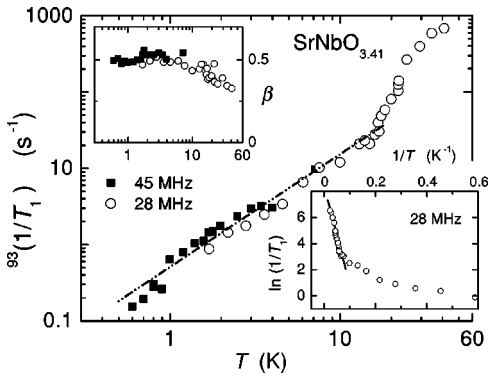

FIG. 5. Logarithmic plot of the ^{93}Nb spin-lattice relaxation rate $1/T_1$ vs T in $SrNbO_{3.41}$ measured at two different frequencies/external fields: (solid squares) 45 MHz/43.2 kOe, (open circles) 28 MHz/26.9 kOe. The dashed line indicates a power law $1/T_1 \propto T^{3/2}$ to guide the eye (see text). Upper inset: stretching exponent β vs ln T. Lower inset: Arrhenius plot of the powder data (28 MHz). The solid line represents a fit $1/T_1 \propto \exp(-\Delta_{\mathrm{NMR}}/k_B T)$; $\Delta_{\mathrm{NMR}} = 6.5$ meV.

As with the spin-spin relaxation time T_2, the spin-lattice relaxation time T_1 for the different stimulating frequencies, i.e., 28 and 45 MHz, appears to be slightly faster at the higher frequency. At present, the origin of this frequency dependence is not clear. For $1/T_1(T)$, two distinct temperature regimes can be identified: At elevated temperatures $15<T<41$ K the temperature dependence of $1/T_1$ exhibits an activated behavior which could be fitted using $1/T_1 \propto \exp(-\Delta_{\mathrm{NMR}}/k_B T)$. In order to demonstrate this behavior we utilize an Arrhenius plot as it is given in the lower inset of Fig. 5. The solid line yields an energy gap of $\Delta_{\mathrm{NMR}} = 6.5$ meV. At first glance, the low temperature regime $1<T<15$ K can be represented by a power law dependence $1/T_1 \propto T^{3/2}$ (dashed line in Fig. 5). This behavior reminds one of the temperature dependence of the host spin-lattice relaxation rate $^{29}(1/T_1)$ in semiconducting Si(B).[19] However, a closer inspection of the low temperature data down to 600 mK reveals a temperature dependence which is indicative for a variable range hopping process (see Fig. 9 in Sec. III.).

C. ELECTRON PARAMAGNETIC RESONANCE

The EPR experiments have been performed at a Bruker ELEXSYS E500-CW spectrometer at *X*-band frequency (9.5

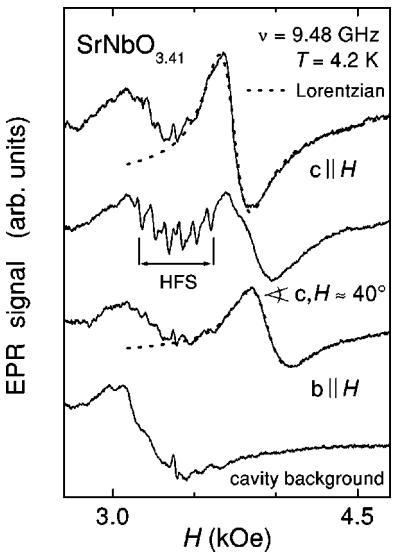

FIG. 6. EPR spectra in $SrNbO_{3.41}$ at three different orientations and background of the cavity at 4.2 K.

GHz). For cooling the sample, we used a continuous He-gas-flow cryostat (Oxford Instruments) at temperatures above 4.2 K and a cold-finger ^{4}He-bath cryostat (Isotherm) in the temperature range $1.7 \leqslant T \leqslant 4.2$ K. The single crystalline sample with dimensions $l_a \times l_b \times l_c$, i.e., $3 \times 2 \times 0.5$ mm^3, was fixed in paraffin within a glass tube. The normal of its cleavage plane corresponds to the crystallographic *c* axis. By means of a Laue diffractogram, the *a* axis was found to be parallel to the longest edge of the rectangular shaped cleavage plane of the crystal. Orientation dependent measurements with respect to the static magnetic field *H* were performed in both the *a*,*b* and the *b*,*c* plane. Due to the lock-in technique with 100 kHz modulation of the static field, the EPR spectra record the field derivative of the microwave power dP_{abs}/dH absorbed by the sample from the magnetic microwave field which is applied perpendicular to the static field.

An EPR response of $SrNbO_{3.41}$ was detectable only at low temperatures $T < 25$ K. Figure 6 shows typical spectra at 4.2 K for three different orientations of the crystal. The spectrum exhibits a well defined resonance line with a weak angular dependence. The low-field wing of the resonance is strongly distorted due to the inevitable background of the cavity which is also included in Fig. 6. A simple subtraction of the background is not possible, because the *Q* factor of the cavity is significantly diminished, when the sample is inserted. This indicates a change of the microwave-field distribution in the cavity, which also affects the background. Nevertheless, the high-field wing of the resonance is well separated from the background and therefore yields a satisfying fit by a Lorentzian line (dotted). At intermediate orientation a sixfold hyperfine structure (HFS) appears which is centered at about 3.4 kOe with a distance $\delta H_{\mathrm{HFS}} = 85$ Oe between neighboring lines. This part of the spectrum follows a Curie law in its intensity and is therefore independent of the main resonance line which behaves in a completely different way as will be discussed below.

The hyperfine structure belongs to an impurity ion with a nuclear spin $I = 5/2$, which gives rise to a $(2I+1=6)$-fold splitting of the respective paramagnetic resonance transition. The magnitude of the splitting is characteristic for ^{55}Mn.[20] Manganese usually attains valence states $2+, 3+$, or $4+$. In the present structure it is probably incorporated at the Nb site as Mn^{4+} (note that Mn^{2+} found in the starting materials can further be oxidized during the preparation process). As the structure contains three inequivalently distorted NbO_6 octahedra,[5] the HFS is smeared out for most of the orientations by the additional influence of the nonuniform crystal electric field. For the angle, where the HFS is observable, the magnetic field is approximately parallel to one of the main axes of all three octahedra yielding a nearly uniform contribution.

It turned out that the intensity of the EPR spectra was much weaker for the magnetic microwave field *h* applied perpendicular to the *a*,*b* plane than perpendicular to the *b*,*c* plane. This observation can be explained by the skin effect due to the strongly anisotropic conductivity. Generally, the skin depth δ of the microwave field can be estimated by

$$\delta = (\rho/\mu_0\omega)^{0.5} \tag{6}$$

from the electric resistance ρ and the microwave frequency $\omega = 2\pi \times 9$ GHz($\mu_0 = 4\pi \times 10^{-7}$Vs/Am). The dc resistivity was found to amount about $\rho_a : \rho_b : \rho_c = 10^{-3} : 10^{-1} : 10^{2}\,\Omega$ cm at low temperatures.[2,3] For the magnetic microwave field *h* oscillating parallel to the *a* axis, circular shielding currents are induced on the surfaces along *b* and *c* directions. The effective resistance can be estimated as $R \propto l_b \cdot \rho_b + l_c \cdot \rho_c$, where l_b and l_c denote the sample dimensions along *b* and *c* direction, respectively. The sample dimensions are of comparable magnitude, whereas the resistivities differ by a factor of 10^3. Therefore, the skin depth is determined by ρ_c alone and can be estimated from Eq. (6) as $\delta(h \| a) \approx 4$ mm. This is larger than the sample thickness and the microwave is probing the full volume of the sample. For the magnetic microwave field *h* applied parallel to the *c* axis, the skin depth is analogously determined by ρ_b as $\delta(h \| c) \approx 0.1$ mm, a value clearly below the sample dimensions. In this case the skin effect is strongly shielding the sample, and the EPR signal originates only from the region near the sample surface.

We now return to the temperature dependence of the main resonance line which can be evaluated up to 20 K. As the asymmetry of the line shape increases with increasing temperature, we fitted the signal by the Dysonian line shape[21]

$$\frac{d}{dH}P_{\mathrm{abs}} = A\frac{-2x + \alpha(1-x^2)}{(1+x^2)^2}, \tag{7}$$

where $x = (H - H_{\mathrm{res}})/\Delta H$. The fit parameters $H_{\mathrm{res}}, \Delta H$, and *A* denote resonance field, half-width at half-maximum of the resonance line and amplitude, respectively. The dispersion-to-absorption ratio α measures the asymmetry of the line shape due to the admixture of the real part of the dynamic susceptibility χ' (dispersion) to the imaginary part χ'' (absorption): It vanishes in insulators yielding a pure Lorentzian

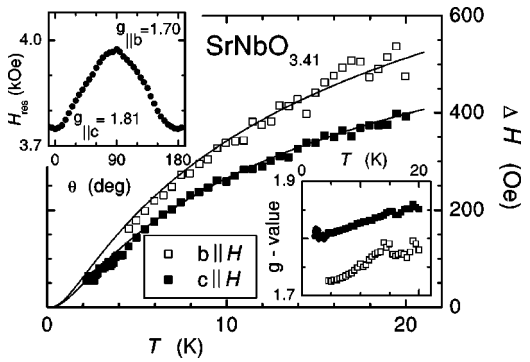

FIG. 7. EPR line width ΔH as a function of temperature for the static magnetic field applied parallel to the c axis (solid symbols) and parallel to the b axis (open symbols), respectively. Solid lines are fits $\Delta H \propto \exp[-(T_0/T)^{1/2}]$ (see Sec. III.). Upper inset: angular dependence of the resonance field within the bc plane. Lower inset: temperature dependence of $g_{\|b}$ and $g_{\|c}$.

shape. But α becomes nonzero in metals, where the skin effect drives the electric and magnetic components of the microwave field out of phase.

Temperature dependencies of the line width and the resonance field obtained from the EPR spectra using Eq. (7) are shown in Fig. 7. At 4.2 K the resonance field $H_{\rm res}$ is found at 3.95 kOe for $H\|b$ and 3.75 kOe for $H\|a, H\|c$, respectively (see upper inset in Fig. 7). Expressing the Larmor frequency as $h\nu = g\mu_B H_{\rm res}$, this corresponds to g values $g_b = 1.70$ and $g_a = g_c = 1.81$, respectively. With increasing temperature the g values shift towards higher values. The difference with respect to the free electron value $g = 2$ decreases by about 30% going from 2 to 20 K. The resonance line width monotonically increases with increasing temperature from 60 Oe at 2 K up to 400 Oe at 20 K.

Figure 8 shows the temperature dependence of the EPR intensity determined by

$$I = A \cdot \Delta H^2 (1 + \alpha^2)^{0.5} \tag{8}$$

For $\alpha = 0$ this is the twofold integral of the field derivative of the pure Lorentzian line. In the case of nonvanishing α, this has to be corrected due to the rotation in the complex plane

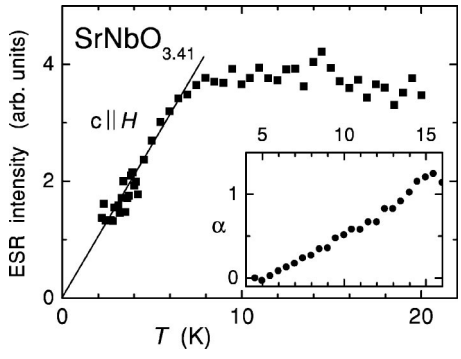

FIG. 8. Temperature dependence of the EPR intensity of the main resonance in $SrNbO_{3.41}$ for $c\|H$. Inset: dispersion-to-absorption ratio α which is a direct measure of the metallicity of the sample.

of the dynamic susceptibility. However, this correction only holds true, if the microwave field can penetrate the whole sample. As soon as the skin depth becomes small compared to the sample dimension, only the spins near the sample surface contribute to the signal. For this reason we determined the intensity for the microwave field h applied parallel to the a axis, where the resistivity in the c direction governs the skin depth, as explained above. The experimentally observed dispersion-to-absorption ratio α is sketched in the inset of Fig. 8. It exhibits a monotonous increase from $\alpha = 0$ at 4 K to $\alpha = 1$ at 15 K. This indicates the increasing conductivity of the sample in accordance with the resistivity measurements reported in Refs. 2,3. For low temperatures the intensity shows an approximately linear increase on temperature and reaches saturation at about 7 K. Above 20 K the line width becomes too large to be reasonably evaluated.

III. DISCUSSION AND CONCLUSION

The magnetic susceptibility χ at elevated temperatures is satisfactorily described in terms of one-dimensional $S = 1/2$ Heisenberg spin chain.[12] Although this model is based on localized spins, this is not in contradiction to conducting behavior. The organic semiconductor $(TMTTF)_2PF_6$ can be taken as paradigm of a localized spin chain with the well known Bonner-Fisher-type susceptibility exhibiting a broad maximum at about 350 K. For the isostructural one-dimensional organic conductor $(TMTSF)_2PF_6$ the temperature dependence of the susceptibility looks quite similar, but the characteristic maximum is shifted at least to temperatures above 500 K beyond the published data.[22] This was explained using the generalized model of Seitz and Klein[23] which admits a certain degree of delocalization within the spin chains. As the resistivity in $SrNbO_{3.41}$ shows a comparable anisotropy and magnitude such as $(TMTSF)_2PF_6$, it seems reasonable to apply this scenario of one-dimensional spin chains.

For temperatures lower than 200 K the susceptibility $\chi(T)$ might be approximated by an activated behavior. For this activated behavior [see Eq. (1)] an energy gap of $E_g = 19.8$ meV is found. It is of the order of magnitude as the activation gap of 38 meV (for $125 < T < 190$ K) which was deduced from resitivity data along the c axis.[3] However, the fit utilizing Eq. (1) bears difficulties concerning the too small diamagnetic contribution and the nonzero Curie-Weiss temperature of the impurity contribution. The latter contribution prohibits the analysis of the intrinsic bulk susceptibility and masks a possible phase transition.

A closer inspection of the local susceptibility is provided by magnetic resonance experiments. In the NMR experiment performed on the powder sample, we observe an activated behavior of the spin-lattice relaxation rate with an energy gap of $\Delta_{\rm NMR} = 6.5$ meV within the temperature range $15 < T < 41$ K. This is in rough agreement with a gap observed along the a axis below $T < 50$ K in resisitivity measurements (6.6 meV), in optical spectroscopy (≈ 5 meV), and in angle-resolved photoemission (≈ 8 meV).[2,3] This gap was discussed in terms of a Peierls scenario and a 1D Mott-Hubbard model at 1/3 band filling.[2] At temperatures $T < 15$ K, the ^{93}Nb spin-lattice relaxation rate in $SrNbO_{3.41}$ reveals a temperature dependence similar to the ^{29}Si rate in boron doped

silicon.[19] This is an important hint towards the presence of acceptor states also in $SrNbO_{3.41}$ which turned out to be a necessary point in order to explain the EPR results.

To understand the origin of the observed EPR line, the temperature evolution of its intensity is of crucial importance. It does not show any Curie-like behavior, as it is usually observed in the case of paramagnetic defects, but it vanishes approaching zero temperature. Hence, this signal cannot be assigned to the low-temperature Curie-Weiss tail of the static susceptibility. Considering the g values only, one might ascribe the resonance line to Nb^{4+} with $4d^1$ electronic configuration. The g shift to values lower than 2 is typical for ions with less than half filled d shell.[20] However, this possibility can be ruled out, because such localized Nb^{4+} spins are expected to show a Curie law in the intensity, as well.

We ascribe the EPR signal to acceptor states located a few Kelvin above the valence band of the semiconducting ground state. At zero temperature, these states are empty and no paramagnetic resonance can be detected. With increasing temperature the acceptor states are filled by thermal activation from the valence band, giving rise to an increasing EPR intensity. When all acceptor states are filled, the intensity reaches saturation and should finally follow a Curie law at higher temperatures, which is not observable any more due to the limited temperature range where the signal is resolved.

The temperature dependence of the acceptor EPR line width (Fig. 7) nicely resembles the findings of the dielectric measurements along the c direction[9] which revealed a temperature dependence of the electrical conductivity $\sigma(T) \propto \exp[-(T_0/T)^{1/2}]$ at temperatures $T<100$ K. This characteristic temperature dependence is typical of two different scenarios: Either one-dimensional hopping in contrast to the well known three-dimensional hopping $\sigma(T)\propto \exp[-(T_0/T)^{1/4}]$,[26,27] or three-dimensional hopping in the presence of a Coulomb gap.[28] At present, it is not possible to decide between the two scenarios in the case of $SrNbO_{3.41}$.

This coincidence of EPR and conductivity measurements is often observed in systems with hopping conductivity,[24] e.g., in calcium doped lanthanum manganites the hopping motion of small polarons was identified by the similar temperature dependence of the two quantities.[25] As it is clearly to be seen in Fig. 9, also the nuclear relaxation rate exhibits the same temperature dependence below $T\approx 15$ K even down to 600 mK rather than the power law proposed above. From the experimental point of view, the nuclear relaxation appears to be governed by the same electron motion. Hence, we suggest this variable-range hopping mechanism also to account for the host NMR spin-lattice relaxation in Si(B) as reported by Fuller *et al.* in Ref. 19.

It is worthy to note that the EPR line width in $SrNbO_{3.41}$ is governed by the spin-lattice relaxation rather than spin-spin relaxation. In analogy to the manganites mentioned above, we assume a tremendous bottleneck situation due to strong coupling between the acceptor and hole states which relax to the lattice very slowly via tunneling processes of the hole states.

Turning to elevated temperatures the characteristics of variable range hopping in $SrNbO_{3.41}$ disappear in favor of the activated behavior for $^{93}(1/T_1)$ which was found to agree

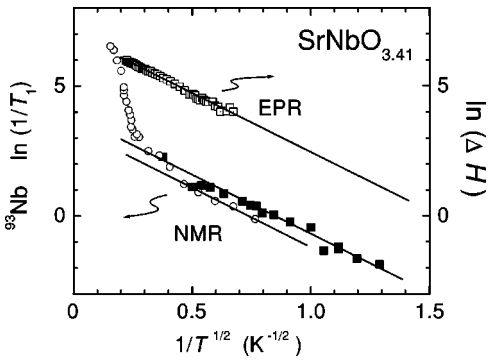

FIG. 9. Plot of the relaxation rates obtained from magnetic resonance experiments ^{93}Nb NMR and EPR, respectively. The spin-lattice relaxation rate $\ln(1/T_1)$ vs $1/T^{1/2}$ in $SrNbO_{3.41}$ measured at two different frequencies/external fields: (solid squares) 45 MHz/43.2 kOe, (open circles) 28 MHz/26.9 kOe.

with the activation of electrons into the conduction band deduced from resistivity measurements, optical spectroscopy, and angle-resolved photoemission. Simultaneously, the EPR signal vanishes presumably due to the opening of the bottleneck by an exponential increase of both electron and hole states which additionally corroborates the existence of this gap also from EPR results.

In conclusion, the bulk susceptibility can be interpreted as arising from almost localized spins in a 1D Heisenberg chain with an exchange constant of $J=530$ K. This proposal has to be checked by high-temperature susceptibility measurements. Another interpretation would be in terms of activated charge carriers across a gap of approximately 20 meV which corresponds to an average value over all crystallographic directions. From the NMR experiments in the intermediate temperature range we deduce a gap of $\Delta_{NMR}=6.5$ meV in agreement with recent resistivity measurements, optical spectroscopy, and angle-resolved photoemission.[2,3] In the bulk susceptibility this gap is masked by the Curie tail of paramagnetic impurities. At present, based on experimental facts it is hard to decide, whether this gap in the electronic density of states is built via the formation of a CDW or if $SrNbO_{3.41}$ has to be characterized as a narrow-gap semiconductor. Due to the one-dimensional structure and susceptibility, an interpretation in terms of CDW ground state such as in $NbSe_3$ cannot be ruled out. Indeed, several observations bear the characteristics of the prototypical CDW compound $NbSe_3$: For $NbSe_3$ the formation of a CDW below the Peierls transition at 145 K affects the nuclear quadrupole interaction in the same way, evolving a huge quadrupole broadening below 40 K (see the inset of Fig. 2) which might be the analogous transition temperature in case of $SrNbO_{3.41}$.[14] Also the energy gap $\Delta_{NMR}=6.5$ meV deduced from the spin-lattice relaxation rate $1/T_1$ corresponds to a correlation induced transition at $T_C\approx 43$ K predicted by mean-field theory $(2\Delta_{NMR}=3.5k_BT_C)$.[29] Additionally, we observe a similar anomaly in the spin-spin relaxation rate $1/T_2$ around the metal-to-semiconductor transition temperature at $T\approx 40$ K in $SrNbO_{3.41}$ as it was reported for $NbSe_3$.[14] More experiments focusing on an expected phase transition around 40 K, especially heat capacity measurements are highly needed to clarify the ground state of $SrNbO_{3.41}$.

ACKNOWLEDGMENTS

We kindly acknowledge D. Vieweg for SQUID measurements, A. Herrnberger for performing Laue diffractograms, and A. Gerashenko who let us have his program for NMR spectra simulations. This work was supported by the BMBF under Contract Nos. 13N6917, 13N6918/1 (EKM), and partly by the Deutsche Forschungsgemeinschaft (DFG) via the Sonderforschungsbereich 484 (Augsburg).

[1] C.A. Kuntscher, S. Gerold, N. Nücker, T.R. Cummins, D.-H. Lu, S. Schuppler, C.S. Gopinath, F. Lichtenberg, J. Mannhart, and K.-P. Bohnen, Phys. Rev. B **61**, 1876 (2000).

[2] C. A. Kuntscher, S. Schuppler, P. Haas, B. Gorshunov, M. Dressel, M. Grioni, F. Lichtenberg, A. Herrnberger, F. Mayr, and J. Mannhart (unpublished).

[3] F. Lichtenberg, A. Herrnberger, K. Wiedenmann, and J. Mannhart, Prog. Solid State Chem. **29**, 1 (2001).

[4] F. Lichtenberg, T. Williams, A. Reller, D. Widmer,and J.G. Bednorz, Z. Phys. B: Condens. Matter **84**, 369 (1991).

[5] S.C. Abrahams, H.W. Schmalle, T. Williams, A. Reller, F. Lichtenberg, D. Widmer, J.G. Bednorz, R. Spreiter, C. Bossard, and P. Günter, Acta Crystallogr., Sect. B: Struct. Sci. **54**, 399 (1998).

[6] S. Nanamatsu, M. Kimura, and T. Kawamura, J. Phys. Soc. Jpn. **38**, 817 (1975).

[7] Y. Akishige, M. Kobayashi, K. Ohi, and E. Sawaguchi, J. Phys. Soc. Jpn. **55**, 2270 (1986).

[8] C.A. Kuntscher, Ph. D. thesis, University of Karlsruhe, 2000.

[9] V. Bobnar, P. Lunkenheimer, J. Hemberger, A. Loidl, F. Lichtenberg, and J. Mannhart (unpublished).

[10] Landoldt-Börnstein, New Series, Group II, Vol. 8, Pt. 1 (Springer-Verlag, Berlin, 1976), p. 27.

[11] G.C. Carter, L.H. Bennett, and D.J. Kahan, Prog. Mater. Sci. 20, P I (1977).

[12] J.C. Bonner and M.E. Fisher, Phys. Rev. **135**, A640 (1964).

[13] W.E. Estes, D.P. Gawel, W.E. Hatfield, and D. Hodgson, Inorg. Chem. **17**, 1415 (1978).

[14] B.H. Suits and C.P. Slichter, Phys. Rev. B **29**, 41 (1984); J.H. Ross, Jr., Z. Wang, and C.P. Slichter, *ibid.* **41**, 2722 (1990).

[15] J. Shi and J.H. Ross, Jr., Phys. Rev. B **45**, 8942 (1992).

[16] W.W. Simmons, W.J. O'Sullivan, and W.A. Robinson, Phys. Rev. **127**, 1168 (1962).

[17] The case $\eta \neq 0$ is explicitly analyzed in J. Chepin and J.H. Ross, Jr., J. Phys.: Condens. Matter **3**, 8103 (1991): if the nuclear Larmor frequency ω_0 exceeds about four times ν_Q, the standard NMR results in Eq. (4) for an inverted central transition, which are only valid in the case of axial symmetry $\eta = 0$, can be utilized.

[18] I.P. Goudemond, J.M. Keartland, M.J.R. Hoch, and G.A. Saunders, Phys. Rev. B **56**, R8463 (1997).

[19] S.E. Fuller, E.M. Meintjes, and W.W. Warren, Jr., Phys. Rev. Lett. **76**, 2806 (1996).

[20] A. Abragam and B. Bleaney, *Electron Paramagnetic Resonance of Transition Ions* (Clarendon Press,Oxford, 1970).

[21] S.E. Barnes, Adv. Phys. **30**, 801 (1981).

[22] M. Dumm, A. Loidl, B.W. Fravel, K.P. Starkey, L.K. Montgomery, and M. Dressel, Phys. Rev. B **61**, 511 (2000); M. Dumm, M. Dressel, A. Loidl, B.W. Frawel, K.P. Starky, and L.K. Montgomery, Synth. Met. **103**, 2068 (1999).

[23] W.A. Seitz and D.J. Klein, Phys. Rev. B **9**, 2159 (1974).

[24] O. Chauvet, T. Stoto, and L. Zuppiroli, Phys. Rev. B **46**, 8139 (1992).

[25] A. Shengelaya, Gou-meng Zhao, H. Keller, K.A. Müller, and B.I. Kochelaev, Phys. Rev. B **61**, 5888 (2000).

[26] N.F. Mott and E.A. Davis, *Electronic Processes in Non-Crystalline Materials* (Clarendon Press, Oxford, 1979).

[27] S. Kagoshima, H. Nagasawa, and T. Sambongi, *One-Dimensional Conductors* (Springer-Verlag, Berlin, 1988), p. 151.

[28] A.L. Efros and B.L. Shklovskii, J. Phys. C **8**, L49 (1975).

[29] C.H. Pennington and C.P. Slichter, in *Physical Properties of High Temperature Superconductor II*, edited by D.M. Ginsberg (World Scientific, Singapore, 1990).